Chapter 6

Preparation of RNA Polymerase Complexes for Their Analysis by Single-Particle Cryo-Electron Microscopy

Michael Pilsl, Florian B. Heiss, Gisela Pöll, Mona Höcherl, Philipp Milkereit, and Christoph Engel

Abstract

Recent technological progress revealed new prospects of high-resolution structure determination of macromolecular complexes using cryo-electron microscopy (cryo-EM). In the field of RNA polymerase (Pol) I research, a number of cryo-EM studies contributed to understanding the highly specialized mechanisms underlying the transcription of ribosomal RNA genes. Despite a broad applicability of the cryo-EM method itself, preparation of samples for high-resolution data collection can be challenging. Here, we describe strategies for the purification and stabilization of Pol I complexes, exemplarily considering advantages and disadvantages of the methodology. We further provide an easy-to-implement protocol for the coating of EM-grids with self-made carbon support films. In sum, we present an efficient workflow for cryo-grid preparation and optimization, including early stage cryo-EM screening that can be adapted to a wide range of soluble samples for high-resolution structure determination.

Key words RNA polymerase I, Preparation of transcription complexes, Single-particle cryo-electron microscopy, Grid preparation, Plunge freezing, Negative staining

1 Introduction

During the past years, development of more sophisticated microscopes, new direct electron detectors, and advances in computational image processing caused a "resolution revolution" [1] in the field of cryo-electron microscopy (cryo-EM). This culminated in the award of the Nobel Prize in Chemistry to three scientists driving these developments: Joachim Frank, Richard Henderson, and Jacques Dubochet in 2017. Recent developments have been summarized in detail [2–8]. With its increasing popularity, the technique is now more easily accessible and widely used in many areas of structural biology research, such as the analysis of transcription complexes [9]. Among many others, cryo-EM studies on RNA polymerase (Pol) I complexes became possible and advanced our understanding of the molecular mechanisms employed by this

Karl-Dieter Entian (ed.), *Ribosome Biogenesis: Methods and Protocols*, Methods in Molecular Biology, vol. 2533, https://doi.org/10.1007/978-1-0716-2501-9_6,

highly specialized enzyme [10–19]. Here, we describe the workflow of biochemical purification and sample preparation of Pol I complexes and the optimization of cryo-grid preparation containing frozen, hydrated single particle specimens with the goal of acquiring high resolution images for structure determination. We focus on grid preparation, quality control, and EM screening in an iterative manner. We also emphasize the steps necessary for establishment of a customized workflow that can be tailored to the needs of any sample suitable for single-particle analysis.

The success of structure determination by single-particle cryo-EM depends on high-quality biochemical preparation and characterization of the molecule(s) of interest. Buffer optimization and stabilization of complexes should be done in the initial phase of a project, strategies are described in detail [20]. We previously presented protocols for the purification of 14-subunit, 590 kDa Pol I complexes and their characterization in vitro [21, 22]. Starting from this, we detail the specimen features which are important for successful structure determination using single-particle cryo-EM and suggest approaches for their optimization. For this purpose, we compare complex preparation- and assembly strategies using endogenously purified Pol I and recombinant transcription factors on nucleic acid templates. Transcription factor complexes can be (a) assembled on a biotinylated DNA, enriched using the interaction with bead-coupled streptavidin and eluted with restriction enzymes [23]. Alternatively (b), size exclusion chromatography (SEC) may yield homogenous and stable complexes that are well-suited for cryo-grid preparation. Large macromolecules can also be enriched using density gradient centrifugation protocols (c). As such, the gradient-fixation (GraFix)-method relies on a sedimentation step coupled with an intra- and intermolecular cross-linking step combining purification and complex stabilization [24, 25]. Following GraFix, a buffer exchange is required to remove sucrose or glycerol that would otherwise interfere with the subsequent freezing process and may increase background noise in cryo-EM images. Generally, cross-linking of protein-protein or protein-nucleic acid complexes can improve their stability during the grid preparation process. This cross-linking can be coupled to a purification step (as in GraFix), or performed directly before grid-plunging (d). These preparation techniques can also be combined, for example, carrying out an SEC run after batch cross-linking. Such a strategy combines the advantages of sample stabilization and purification while directly including the transition to a suitable buffer system but requires larger quantities of sample.

In addition to sample preparation and stabilization, we discuss the use of different grid types and support materials. General cryo-EM sample preparation techniques applicable to a wide range of samples were described in detail [26, 27]. Adsorption of particles to a thin support film can aid sample concentration, alter bias in

orientation distribution, or protect fragile particles from denaturation on air–water interfaces [28]. To this end, grids covered with thin carbon layer substrates are commonly used. Additionally, graphene oxide or hydrogenated graphene were reported to be well-suited support materials as they are almost transparent to electrons [29–31]. While holey carbon grids covered with ultrathin support layers are commercially available (*see* Subheading 2), many support types can be manually prepared more economically at similar or higher quality. We also describe a technical gadget to float an ultrathin carbon film on holey carbon grids. This is similar to other floatation techniques [32], but allows for sample adsorption on precoated grids directly prior to plunging and may thus be helpful to some users. This device is based on [33] and is commercially available in a modified form (SKU 10840; LADD Research Industries, Williston, VT, USA).

In addition to sample optimization and the choice of grid type, various physical parameters influence the preparation of cryo-EM grids. Glow discharge settings, grid type variation, buffer choice, and the mechanics of the blotting device should be carefully considered for each individual sample.

In general, we recommend initial optimization using negative staining EM, followed by two stages of cryo-EM screening (Fig. 1). The first cryo-screening stage aims at an evaluation of grid types, support films, or blotting conditions and gives information on sample behavior in ice. In a second phase of cryo-screening, intermediate-resolution single-particle maps may be reconstructed. Phase I cryo-screening results yield insights into sample behavior, whereas results of the second cryo-screening phase indicate whether the sample is suitable for high-resolution data collection by identifying flexibilities within the macromolecular complex and bias in orientation distribution.

For screening, we recommend the acquisition of low-magnification grid maps for navigation and evaluation of overall ice distribution. Low dose acquisition strategies to avoid beam-induced particle damage are used. This workflow includes focusing and exposure-dose measurement at higher magnifications on grid areas adjacent to the foil-hole of interest using image/beam shift functions, as for the acquisition of high-resolution images. Overviews of sample preparation, the use of cryo-holders and imaging strategies have been described [34–37]. For automated data collection, the SerialEM software includes many more features that have been recently summarized [38]. The open-source software is freely available and can be adapted to a wide range of microscopes and camera systems. Recent developments include the implementation of “on-the-fly” data processing and evaluation strategies into the software packages RELION, Warp, cryoSPARC, and SPHIRE, that may be useful in sample evaluation [39–42]. Here, we focus on the sample and grid preparation, as well as phase I cryo-EM screening approaches for multisubunit RNA polymerases.

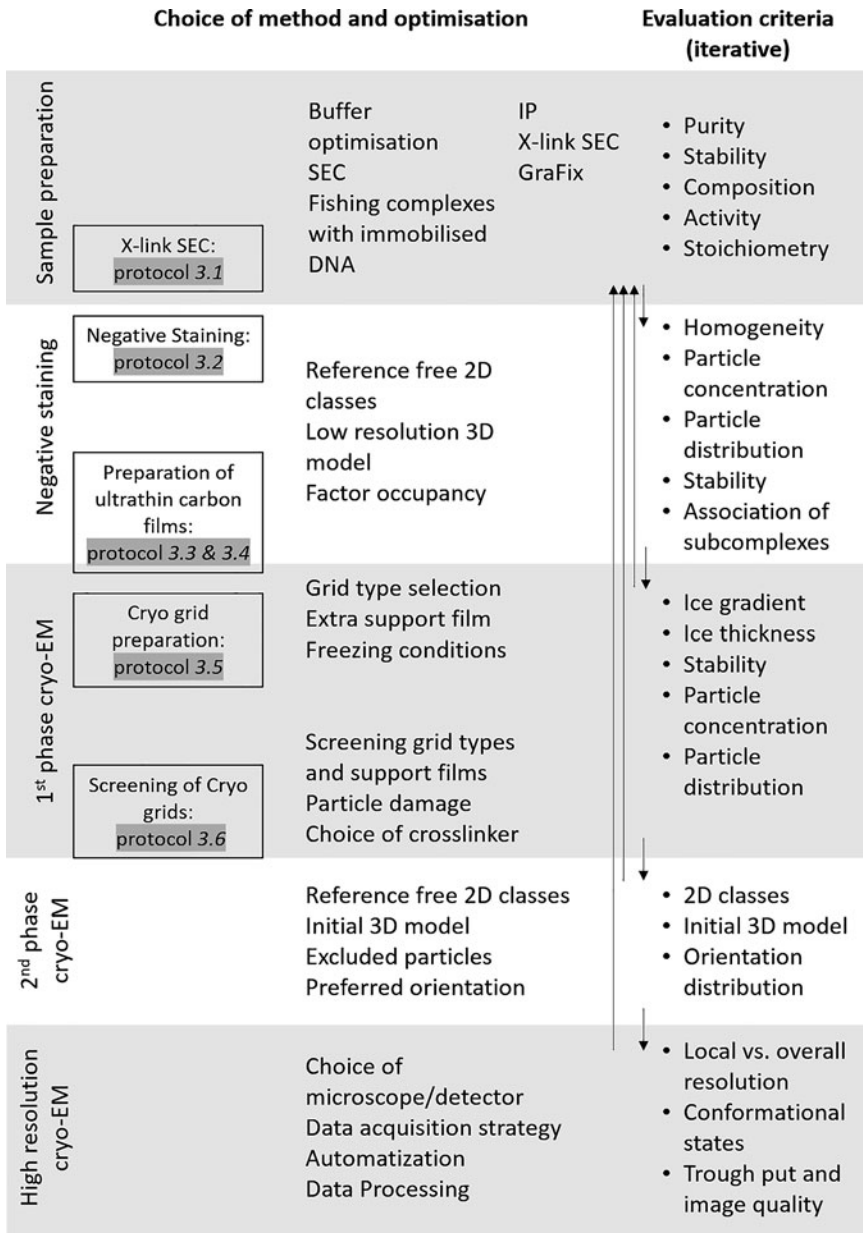

Fig. 1 Overview of a workflow for (cryo-)EM sample screening and grid optimization. We suggest five phases, starting with sample preparation and iterative evaluation of screening results. Detailed protocols for individual steps are referenced and listed in Subheadings 3.1–3.6

2 Materials

2.1 Assembly of Pol I Complexes

2.1.1 Materials

1. Amicon Ultra Concentrators 100 kDa MWCO (Millipore).
2. Superose 6 Increase 3.2/300 column (GE Healthcare).
3. Microvolume FPLC system (e.g., Ettan LC or Aekta Micro; GE Healthcare).
4. Bis(sulfosuccinimidyl)suberate (BS3) crosslinker (Thermo Fisher Scientific).

2.1.2 Buffers

1. Quenching buffer: 2 M ammonium hydrogen carbonate.
2. H0 buffer: 20 mM HEPES–KOH pH 7.8, 5 mM DTT.
3. SEC buffer: 20 mM HEPES–KOH pH 7.8, 150 mM potassium acetate, 1 mM magnesium chloride, 10 μM zinc chloride, 5 mM DTT.

2.2 Negative Staining

2.2.1 Materials

1. Parafilm M (Bemis Flexible Packaging).
2. Uranyl Formate (powder; Science Services).
3. Bidest. water (unfiltered).
4. Filter paper grade 1 (Whatman).
5. Carbon coated EM grid (e.g., Plano S160 or homemade on 300 mesh copper grids).
6. Glow discharge device (Harrick: Plasma Cleaner/Sterilizer PDC-3xG, or Pelco 'EasiGlow' plasma cleaner (Ted Pella), or similar).

2.3 Preparation of Ultrathin Carbon Film Coated Grids

1. Cressington 208 carbon coater (Cressington) or similar.
2. Self-made Floatation device (acrylic glass chamber, foldback binder clip, metal support mesh) (*see* Fig. 2).
3. Carbon rods (6.15 × 305 mm; Elektronen-Optik-Service GmbH).
4. Freshly cleaved mica (Glimmer "V3" 75 × 25 mm; PLANO GmbH).
5. Glass slide (for light microscopy; Menzel-Gläser or similar).
6. Filter paper grade 1 (Whatman).
7. Reverse forceps ('N5'; Dumont).
8. Petri dish (glass; ~90 mm diameter).
9. EM grids (Quantifoil R 2/1 or 2/2).
10. Bidest. water.
11. Glow discharge device, (Harrick: Plasma Cleaner/Sterilizer PDC-3xG).

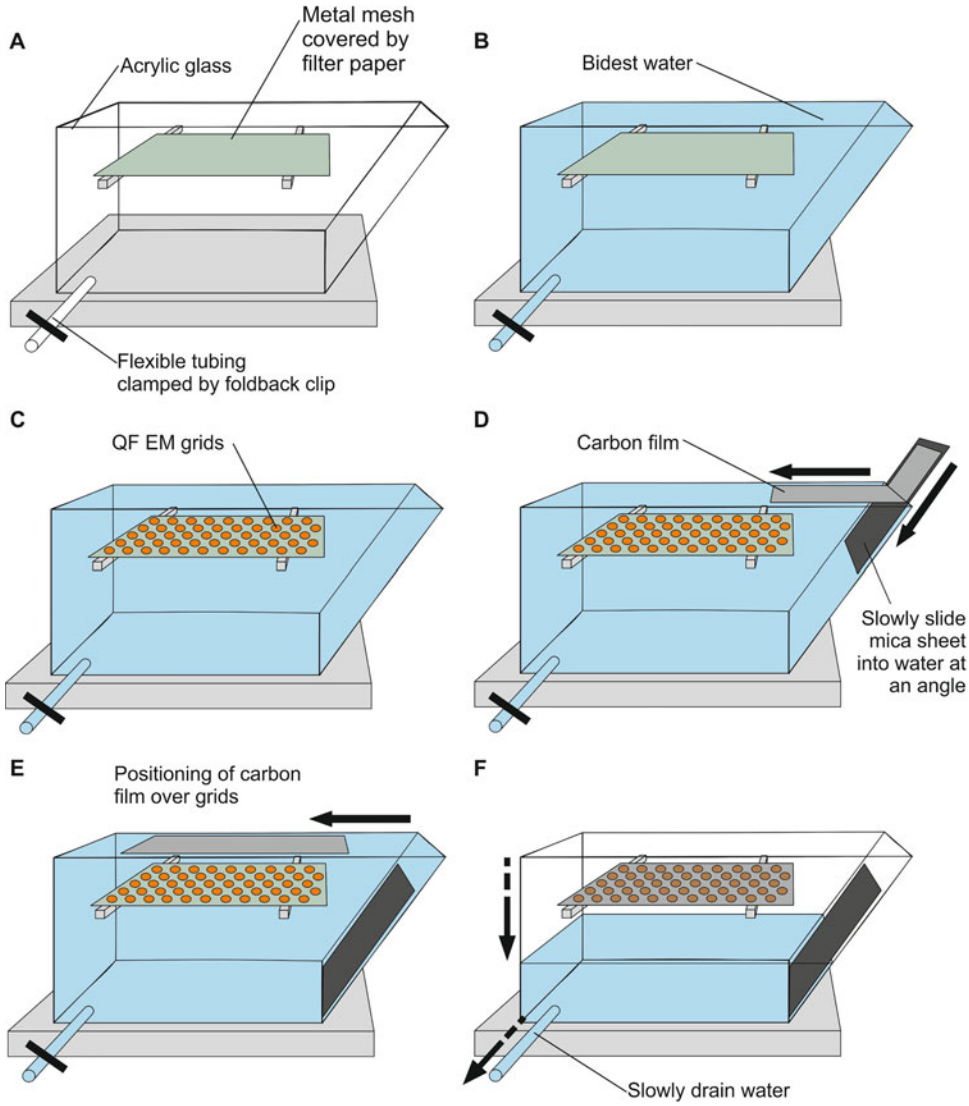

Fig. 2 Schematic representation of carbon film transfer onto EM grids as detailed in Subheading 3.4 (QF: Quantifoil, EM: Electron Microscopy)

2.4 Cryo-Grid Preparation

1. Liquid nitrogen.
2. Ethane (3.5, Linde).
3. EM grids: "R 1.2/1.3" (Quantifoil); "R 2/1" (Quantifoil); "R 2/1 + 2 nm Carbon" (Quantifoil); homemade ultrathin carbon film floated on "R 2/1" (Quantifoil).
4. Cryo grid storage boxes (Plano).
5. Pelco "EasiGlow" plasma cleaner (Ted Pella), or similar.
6. Vitrobot Mark IV (Thermo Fisher Scientific).

2.5 Cryo-Electron Microscopy

1. JEM 2100F (JEOL) operating at 200 kV equipped with a 4 k × 4 k CMOS camera (TemCam-F416, TVIPS GmbH) or similar.
2. Liquid Nitrogen.
3. Gatan 626 Cryo Transfer Holder (Gatan), or similar.
4. Clip Ring (Gatan).
5. Clip Ring Tool (Gatan).
6. SerialEM software package [43].

3 Methods

3.1 Assembly of Pol I Complexes

1. Equilibrate Superose 6 Increase 3.2/300 column with two column volumes (CVs) SEC buffer on micro-volume SEC system.
2. Mix proteins and nucleic acids (stoichiometry, assembly and incubation conditions subject of optimization). We typically load ~100 μg protein to the SEC column for non–cross-linked samples and start with ~200 μg if the complex will be cross-linked before the SEC run.
3. Adjust salt concentration of the assembly reaction with buffer H0 to 150 mM potassium acetate (SEC buffer).
4. Incubate for 30 min at 4 °C (up to 25 °C).
5. Add BS3-crosslinker to a final concentration of 1 mM and incubate for 30 min at 30 °C (*see* **Note 1**).
6. Quench cross-linking reaction with ammonium hydrogen carbonate at a final concentration of 100 mM for 15 min at 30 °C (*see* **Note 2**).
7. Concentrate the sample to a final volume of 20–50 μl using the Amicon Ultra Concentrators 100 kDa MWCO (Millipore) if necessary.
8. Centrifuge sample 5 min at 15,000 × *g* to remove large aggregates. Transfer supernatant to fresh tube.
9. Load sample onto the equilibrated Superose 6 Increase 3.2/300 column and collect 50 μl fractions.
10. Evaluate 260 and 280 nm UV spectra for comigration of nucleic acids, pool peak fractions (*see* **Note 3**).

3.2 Negative Staining

1. Prepare saturated uranyl formate solution: Add ~10–20 mg of uranyl formate in 1.5 ml tube, add 400 μl bidest water, vigorously vortex for 2 min and centrifuge for >10 min at 15,000 × *g* (*see* **Note 4**).
2. Glow discharge EM grid(s) for 30 s.

3. Prepare a drop of 500 µl bidest. Water on a clean surface (Parafilm).
4. Apply 5 µl sample to a freshly glow-discharged, carbon-coated EM grid and adsorb for 30 s (*see* **Note 5**).
5. Wash the grid for 20 s in the droplet of bidest. Water.
6. Add 5 µl of uranyl formate, incubate for 20 s and blot liquid from the edge of the grid (Whatman filter paper). Repeat this step two more times (three staining steps in total) (*see* **Note 6**).
7. Dry grid for >5 min before storage. Grids can be directly imaged or long-term stored in a dry place but must be protected from dust.
8. We evaluate the negative stain image for homogeneity, complex stability, and concentration. Collection of small datasets comprising at least 10,000 negatively stained particles (20–100 images should be sufficient at magnifications of 30,000–50,000×) can be used to calculate initial low-resolution 2D and 3D classes (*see* **Note 7**).

3.3 Preparation of Ultrathin Carbon Film

1. Fix freshly cleaved mica halves on glass slide using small strips of tape on both ends. Slide a piece of filter paper under mica (*see* **Note 8**).
2. Vent and open the carbon coater and place glass slide with mica on stage.
3. Check carbon rods: left rod should have a smooth tip, right rod should have a plain face, both rods have to be in physical contact.
4. Close the recipient chamber. Turn on Cressington carbon coater device and wait for the vacuum to be under 4×10^{-5} mbar.
5. Degas carbon rods: Slowly turn up voltage to 2 V, hold until carbon rod glows red. Wait for vacuum to recover and repeat two more times.
6. Switch on the thickness monitor and evaporate carbon at 3.6 V for 10 s. Do not remove shield to ensure indirect evaporation. Wait at least 30 s before reading the carbon film thickness from the monitor, the film should be ~2 nm. Repeat evaporation if necessary (*see* **Note 9**).
7. Vent the recipient chamber, wait at least 5 min before opening it (evaporation source will become hot during evaporation). Store carbon films on mica carrier for >3 days (ideally >10 days) in a petri dish before use (*see* **Note 10**).

3.4 Carbon Film Transfer onto EM Grids

1. Construct a floatation chamber well in advance (compare Fig. 2). The design was described in [33] and should be adaptable in a scientific workshop. A commercial version (SKU

10840) of a similar apparatus is available from LADD Research Industries (Williston, VT, USA). We also use this flotation chamber to transfer surface assembled graphene oxide [44] onto EM grids.

2. Prepare a sheet of filter paper that is slightly bigger than the carbon film produced in "Preparation of ultrathin carbon film" and mark the rough outline of the carbon film on this filter paper with a pencil.
3. Place metal support mesh on beams in floatation chamber and place marked filter paper on top of metal mesh. Close the flexible outlet tube at the chamber bottom using a clip or connect to peristaltic pump.
4. Fill the chamber with bidest. Water to about 0.5 cm above the filter paper.
5. Carefully place freshly glow-discharged EM grids (30 s on setting "low") on the filter paper (*see* **Note 11**).
6. Pick up the carbon-covered mica sheet (see above) with forceps at a position previously covered by tape (no carbon film).
7. Slowly slide the mica sheet into the water with the carbon film facing upward and monitor carbon film detachment on the surface. Slowly and continuously slide the mica into the water until fully submerged (*see* Fig. 2).
8. Carefully position the floating carbon film on top of the grids using the forceps.
9. Slowly drain the water by opening the clip on the outlet tube and continue to guide the carbon film over the grids.
10. Place the filter paper (with the wet, now coated grids on top) in a petri dish containing an additional filter paper at the bottom. Cover and allow to dry over-night.
11. Check carbon film under binocular reflection microscope: Are holey Quantifoil film and the carbon support on the same side? Only one layer of untorn support must be visible on a grid (this can also be checked in a transmission electron microscope) (*see* **Note 12**).

3.5 Cryo-Grid Preparation

1. Prepare the Vitrobot Mark IV plunge freezer according to manufacturer's instruction (Thermo Fisher): Fill water reservoir of the humidifier with 60 ml water, place new filter papers and cool down humidity chamber of the Vitrobot to 4° for ~45 min. Set humidity to 100% after 30 min and enable the humidifier, to moisten the filter paper (*see* **Note 13**).
2. Check Vitrobot settings and perform a test run without grid or forceps. Vitrobot settings: 4 °C, 100%, Blotting settings: wait 0 s, blot 5 s, drain 0 s, Blot force 12 (*see* **Note 14**).

3. Cool the cryogen container with liquid nitrogen for 5 min.
4. Condense ethane (handle with caution under fume hood, wear eye and skin protection) (*see* **Note 15**).
5. Wait until solid ethane precipitates at the edges of the cryogen container, remove cooling "spider" apparatus and transfer the cryogen-containing assembly to the Vitrobot (*see* **Note 16**).
6. Glow discharge EM grids (carbon side up, if applicable), for holey carbon grids: 2 × 100 s, 15 mA, 0.4 mbar; for grids coated with ultrathin carbon film: 30 s, 15 mA, 0.4 mbar.
7. Label and place grid storage boxes in cavities inside the cooling container.
8. Pick up a freshly glow-discharged grid with the Vitrobot tweezers, be sure you only touch the rim of the grid and mount the tweezers with the grid on the Vitrobot plunging rod.
9. Click "continue" to lift the forceps into the humidity chamber and the Styrofoam nitrogen cup with the cryogen container.
10. Apply 3–5 μl of sample and start the blotting and plunging process (*see* **Note 17**).
11. Once the grid was plunged into the ethane container and automatically retracted from the humidity chamber, carefully slide the tweezer from the plunging rod. Make sure to keep the grid covered with liquid ethane while removing the Styrofoam container from its holder in the Vitrobot (*see* **Note 18**).
12. Transfer the grid from liquid ethane to liquid nitrogen and into the storage box. Close full storage boxes and store in nitrogen at the bottom of the Styrofoam container until transfer to a storage container (*see* **Note 19**).
13. Store grid boxes in a liquid nitrogen tank (*see* **Note 20**).

3.6 Cryo-Electron Microscopy

1. Place Gatan 626 cryo holder in transfer station and fill the transfer station with liquid nitrogen. Fill the holder Dewar (which will keep the specimen cold during the transfer and microscopy process) with liquid nitrogen directly afterward (*see* **Note 21**).
2. Wait for ~15 min until station is equilibrated (nitrogen stops boiling). Optional: Connect the temperature control unit to the holder and confirm stable temperature is around −180 °C.
3. Precool all tweezers and other tools used from here on in liquid nitrogen to avoid heating of the vitreous sample.
4. Transfer EM grid to the slot at the tip of the holder and fix it with the clip ring (*see* **Note 22**).
5. Close the shield over the sample by sliding the lever on the back for the holder Dewar to protect it during grid transfer to the microscope.

Optional: Prepare electron microscope by tilting the stage 30° to avoid spilling liquid nitrogen during holder insertion.

6. Insert holder into the microscope and evacuate the lock. Wait until vacuum recovers.
7. Start SerialEM software [43] and check microscope alignment, low-dose mode settings and imaging states and determine the eucentric height of the specimen (*see* **Note 23**).
8. Create a map of the entire grid at low magnification (80–100×). If using the FEI Vitrobot for plunging, a gradient in ice thickness should be visible. Ice in some regions may be too thick for electrons to pass through and appear black, while regions on the opposite side of the grid may be almost dry.
9. Start the Serial-EM "Navigator" function. Create a map from the atlas and select grid squares with different ice appearance to be screened at higher magnifications. Using the 'add points' feature of the navigator to save coordinates may be helpful.
10. Acquire images at intermediate magnification (2000×) to correlate overall ice appearance with local distribution. Eventually make maps at this intermediate magnification, this could help navigating on the grid-square and is useful, if some more micrographs should be collected.
11. Image areas with distinct ice thickness and distribution. We acquire images at 40,000× magnification (2.7 Å/pixel) using the low dose mode setup in SerialEM, taking focus images at the carbon support foil. Ensure the illuminated area for the focus does not overlap with the area to be imaged. Relying on the calibration of our electron beam we acquire images at 20–50 e^{-}/A^{2}.
12. We evaluate the grid atlas based on ice distribution, to eventually adjust blotting or glow discharge parameters. Higher magnification images are evaluated on sample heterogeneity, stability, behavior of the sample in thinner and thicker ice, and particle concentration and distribution.

4 Notes

1. Optimal concentration of crosslinker can be determined with a titration experiment, depending on temperature and time we suggest 0.1–5 mM for BS3.
2. A short prior quenching with lysine, aspartate or a mixture of amino acids will modify surface properties and could influence orientation distribution.
3. For quality control, we compare cross-linked/non–cross-linked SEC fractions using negative stain EM and SDS-PAGE (silver stain).

4. Solution should have a dark yellow color with precipitation at the bottom of the tube. Optional addition of NaOH drops could improve staining, but also lead to more precipitation.
5. Longer absorption times will increase the particle density, but may lead to evaporation effects (precipitation of salts on grid).
6. Do not blot completely dry, leave a thin film of staining solution on surface of the grid between the staining steps. Particles should be embedded into the heavy metal stain, complete blotting of the stain may introduce artifacts such as positive staining of the particles.
7. Although the resolution will be limited by the stain, one may obtain important information about factor occupancy and particle damage. However, the heavy metal staining at low pH values may introduce artifacts. Therefore, this serves only as a first insight into the quality of your sample.
8. The filter paper serves as internal control whether the coating has worked and also as optical thickness comparison with other batches.
9. The carbon film is not as transparent as alternatives described above, introduces some background signal and might be problematic to use with smaller particles with low intrinsic signal to noise ratio. However, the carbon support works well for Pol I complexes, which have molecular masses of >600 kDa.
10. Carbon films on mica sheets can be stored in petri dishes over years. 2 nm films are used for cryo-grid preparations, thicker films (5–8 nm) can be used for negative staining.
11. Take care that they do not turn; the holey film should face upward. Grids must not overlap.
12. Holy film and carbon will appear shiny, rainbow-like colored; backside should not have this appearance.
13. During the cryo-grid preparation process, surface effects play an important role. The behavior of protein complexes at air–water and grid support–water interfaces can hardly be predicted. Evaporation effects may lead to increasing salt concentrations and surface saturation resulting in protein aggregation [26]. We recommend using low temperatures at 100% humidity as described.
14. We initially used apo ferritin and Pol I [45, 46] to find starting conditions on our Vitrobot. Adaptation of blot force (−20 to +20), wait time (<2 min), sample volumes of 2–8 μl, blotting times from 1 to 10 s, and glow discharge conditions may be worth screening. For our machine and sample types, 5 s blotting at blot force 12 without wait or drain time for a 3 μl sample seem to work well as starting conditions.

15. We hold the tip of the ethane outlet to the lower bottom edge of the ethane container and slowly lift it near the surface of liquid ethane in the pot. A slurping sound will ensure the right flowrate of ethane gas.
16. Liquid ethane is the mostly used cryogen for cryo-grid freezing. The temperature of the cryogen is critical for the vitrification process. At temperatures higher than 133 K (−140 °C), vitreous water will be transformed into cubic or hexagonal ice, the grid is no longer usable. Ethane should be used close to its melting point (90.4 K; −182.8 °C) but is still liquid at higher temperatures (boiling point ethane: 184.6 K; −88.4 °C) not suitable for sample vitrification [47]. To achieve this, we wait until we observe some freezing ethane on edges of the ethane container. However, too much solid ethane can damage grids or forceps. Addition of 10% propane will lower the melting temperature and the cryogen will stay liquid. Alternatively, the use of a cryostat system to control the ethane/cryogen temperature can be an option and applied to most plunge freezing systems [48]. [Boiling point nitrogen: 77.4 K (−195.8 °C), Melting point ethane: 90.4 K (−182.8 °C), Boiling point ethane: 184.6 K (−88.4 °C)].
17. For Cryo-EM grid preparation, only little sample amounts are required. If the sample is adsorbed to a thin carbon film, concentrations as low as 50 ng/μl of sample concentration are sufficient. Even lover amounts can be used in customized humidity chambers if adsorption times are significantly increased [19]. Negative stain quality control is recommended to monitor particle homogeneity and distribution. For preparation of unsupported holey carbon grids, the required sample concentration is 2–5× higher to yield similar particles densities.
18. Use of a face mask may help to prevent surface ice contamination, as nitrogen atmosphere will not be disturbed. Avoid contact of ice-covered tools with liquid nitrogen or ethane to prevent sample contamination.
19. Even though the procedure is not fully reproducible in our hands, the blotting procedure introduces a gradient and the method is robust enough to generate vitrified ice of different quality. Depending on grid types, high-resolution data collection usually requires no more than 20 squares with suitable ice.
20. Visible ethane contamination on the grid surface will sublimate within one or two days of storage in liquid nitrogen tank. During storage, ice flakes in the liquid nitrogen may start contaminating your grids. Thus, we use cryo-grids no longer than 3 months following plunging.

21. Measures to reduce ice contamination may be helpful: Work should be carried out in a low-humidity environment. A protective mask can be worn. Dewars should be covered with lids while equilibrating. Start filling of liquid nitrogen at the tip of the holder, then the Dewar, to avoid ice formation at the specimen tip. Each tool used should be heated and dried after use in nitrogen.
22. First-time users may practice at room temperature and with empty grids first.
23. Our screening workflow is highly compatible with the SerialEM software package. We recommend setup of the low-dose mode to avoid exposure-induced damage by unnecessary illumination of the sample. The software is freely available, constantly updated and can be adapted to most microscopes and cameras.

Acknowledgments

We thank Herbert Tschochner and Joachim Griesenbeck for discussions, Lena Heuschneider for technical assistance, and Reinhard Rachel for practical advice. We acknowledge funding by SFB960 of the DFG (TP-A8 to CE and TP-B1 to PM) and by the "Emmy-Noether-Programme" (DFG grant no. EN 1204/1-1 to CE).

References

1. Kühlbrandt W (2014) Biochemistry. The resolution revolution. Science 343:1443–1444. https://doi.org/10.1126/science.1251652
2. Callaway E (2015) The revolution will not be crystallized: a new method sweeps through structural biology. Nature 525:172–174. https://doi.org/10.1038/525172a
3. Vinothkumar KR, Henderson R (2016) Single particle electron cryomicroscopy: trends, issues and future perspective. Q Rev Biophys 49:e13. https://doi.org/10.1017/S0033583516000068
4. Fernandez-Leiro R, Scheres SHW (2016) Unravelling biological macromolecules with cryo-electron microscopy. Nature 537:339–346. https://doi.org/10.1038/nature19948
5. Frank J (2017) Advances in the field of single-particle cryo-electron microscopy over the last decade. Nat Protoc 12:209–212. https://doi.org/10.1038/nprot.2017.004
6. Lyumkis D (2019) Challenges and opportunities in cryo-EM single-particle analysis. J Biol Chem 294:5181–5197. https://doi.org/10.1074/jbc.REV118.005602
7. Nogales E (2016) The development of cryo-EM into a mainstream structural biology technique. Nat Methods 13:24–27
8. Glaeser RM (2019) How good can single-particle cryo-EM become? What remains before it approaches its physical limits? Annu Rev Biophys 48:45–61. https://doi.org/10.1146/annurev-biophys-070317-032828
9. Hanske J, Sadian Y, Müller CW (2018) The cryo-EM resolution revolution and transcription complexes. Curr Opin Struct Biol 52:8–15. https://doi.org/10.1016/j.sbi.2018.07.002
10. Pilsl M, Crucifix C, Papai G, Krupp F, Steinbauer R, Griesenbeck J, Milkereit P, Tschochner H, Schultz P (2016) Structure of the initiation-competent RNA polymerase I and its implication for transcription. Nat Commun 7:12126. https://doi.org/10.1038/ncomms12126
11. Engel C, Plitzko J, Cramer P (2016) RNA polymerase I–Rrn3 complex at 4.8 Å resolution. Nat Commun 7:12129. https://doi.org/10.1038/ncomms12129

12. Engel C, Gubbey T, Neyer S, Sainsbury S, Oberthuer C, Baejen C, Bernecky C, Cramer P (2017) Structural basis of RNA polymerase I transcription initiation. Cell 169:120–131. e22. https://doi.org/10.1016/j.cell.2017.03.003
13. Tafur L, Sadian Y, Hoffmann NA, Jakobi AJ, Wetzel R, Hagen WJH, Sachse C, Müller CW (2016) Molecular structures of transcribing RNA polymerase I. Mol Cell 64:1135–1143. https://doi.org/10.1016/j.molcel.2016.11.013
14. Neyer S, Kunz M, Geiss C, Hantsche M, Hodirnau V-V, Seybert A, Engel C, Scheffer MP, Cramer P, Frangakis AS (2016) Structure of RNA polymerase I transcribing ribosomal DNA genes. Nature 540:607–610. https://doi.org/10.1038/nature20561
15. Heiss FB, Daiß JL, Becker P, Engel C (2021) Conserved strategies of RNA polymerase I hibernation and activation. Nat Commun 12:758. https://doi.org/10.1038/s41467-021-21031-8
16. Pilsl M, Engel C (2020) Structural basis of RNA polymerase I pre-initiation complex formation and promoter melting. Nat Commun 11:1206. https://doi.org/10.1038/s41467-020-15052-y
17. Torreira E, Louro JA, Pazos I, González-Polo N, Gil-Carton D, Duran AG, Tosi S, Gallego O, Calvo O, Fernández-Tornero C (2017) The dynamic assembly of distinct RNA polymerase I complexes modulates rDNA transcription. elife 6:e20832. https://doi.org/10.7554/eLife.20832
18. Sanz-Murillo M, Xu J, Belogurov GA, Calvo O, Gil-Carton D, Moreno-Morcillo M, Wang D, Fernández-Tornero C (2018) Structural basis of RNA polymerase I stalling at UV light-induced DNA damage. Proc Natl Acad Sci U S A 115:8972–8977. https://doi.org/10.1073/pnas.1802626115
19. Han Y, Yan C, Nguyen THD, Jackobel AJ, Ivanov I, Knutson BA, He Y (2017) Structural mechanism of ATP-independent transcription initiation by RNA polymerase I. elife 6:e27414. https://doi.org/10.7554/eLife.27414
20. Stark H, Chari A (2016) Sample preparation of biological macromolecular assemblies for the determination of high-resolution structures by cryo-electron microscopy. Microscopy (Oxf) 65:23–34. https://doi.org/10.1093/jmicro/dfv367
21. Engel C (2016) Purification of crystallization-grade RNA polymerase I from S. cerevisiae. Methods Mol Biol 1455:85–97. https://doi.org/10.1007/978-1-4939-3792-9_7
22. Pilsl M, Merkl PE, Milkereit P, Griesenbeck J, Tschochner H (2016) Analysis of *S. cerevisiae* RNA polymerase I transcription in vitro. Methods Mol Biol 1455:99–108. https://doi.org/10.1007/978-1-4939-3792-9_8
23. He Y, Fang J, Taatjes DJ, Nogales E (2013) Structural visualization of key steps in human transcription initiation. Nature 495:481–486. https://doi.org/10.1038/nature11991
24. Kastner B, Fischer N, Golas MM, Sander B, Dube P, Boehringer D, Hartmuth K, Deckert J, Hauer F, Wolf E, Uchtenhagen H, Urlaub H, Herzog F, Peters JM, Poerschke D, Lührmann R, Stark H (2008) GraFix: sample preparation for single-particle electron cryomicroscopy. Nat Methods 5:53–55. https://doi.org/10.1038/nmeth1139
25. Stark H (2010) GraFix: stabilization of fragile macromolecular complexes for single particle cryo-EM. Methods Enzymol 481:109–126
26. Passmore LA, Russo CJ (2016) Specimen preparation for high-resolution Cryo-EM. Methods Enzymol 579:51–86. https://doi.org/10.1016/bs.mie.2016.04.011
27. Thompson RF, Walker M, Siebert CA, Muench SP, Ranson NA (2016) An introduction to sample preparation and imaging by cryo-electron microscopy for structural biology. Methods 100:3–15. https://doi.org/10.1016/j.ymeth.2016.02.017
28. D'Imprima E, Floris D, Joppe M, Sánchez R, Grininger M, Kühlbrandt W (2019) Protein denaturation at the air-water interface and how to prevent it. elife 8:e42747. https://doi.org/10.7554/eLife.42747
29. Pantelic RS, Meyer JC, Kaiser U, Baumeister W, Plitzko JM (2010) Graphene oxide: a substrate for optimizing preparations of frozen-hydrated samples. J Struct Biol 170:152–156. https://doi.org/10.1016/j.jsb.2009.12.020
30. Pantelic RS, Suk JW, Magnuson CW, Meyer JC, Wachsmuth P, Kaiser U, Ruoff RS, Stahlberg H (2011) Graphene: substrate preparation and introduction. J Struct Biol 174:234–238. https://doi.org/10.1016/j.jsb.2010.10.002
31. Russo CJ, Passmore LA (2014) Controlling protein adsorption on graphene for cryo-EM using low-energy hydrogen plasmas. Nat Methods 11:649–652. https://doi.org/10.1038/nmeth.2931
32. Göringer HU, Stark H, Böhm C, Sander B, Golas MM (2011) Three-dimensional reconstruction of Trypanosoma brucei editosomes

using single-particle electron microscopy. Methods Mol Biol 718:3–22

33. Dykstra MJ, Reuss LE (2003) Biological electron microscopy. Theory, techniques, and troubleshooting, 2nd edn. Springer US, Boston, MA
34. Grassucci RA, Taylor DJ, Frank J (2007) Preparation of macromolecular complexes for cryo-electron microscopy. Nat Protoc 2:3239–3246. https://doi.org/10.1038/nprot.2007.452
35. Grassucci RA, Taylor D, Frank J (2008) Visualization of macromolecular complexes using cryo-electron microscopy with FEI Tecnai transmission electron microscopes. Nat Protoc 3:330–339. https://doi.org/10.1038/nprot.2007.474
36. Cheng A, Eng ET, Alink L, Rice WJ, Jordan KD, Kim LY, Potter CS, Carragher B (2018) High resolution single particle cryo-electron microscopy using beam-image shift. J Struct Biol 204:270–275. https://doi.org/10.1016/j.jsb.2018.07.015
37. Cheng A, Tan YZ, Dandey VP, Potter CS, Carragher B (2016) Strategies for automated CryoEM data collection using direct detectors. Methods Enzymol 579:87–102. https://doi.org/10.1016/bs.mie.2016.04.008
38. Schorb M, Haberbosch I, Hagen WJH, Schwab Y, Mastronarde DN (2019) Software tools for automated transmission electron microscopy. Nat Methods 16:471–477. https://doi.org/10.1038/s41592-019-0396-9
39. Zivanov J, Nakane T, Forsberg BO, Kimanius D, Hagen WJ, Lindahl E, Scheres SH (2018) New tools for automated high-resolution cryo-EM structure determination in RELION-3. elife 7:e42166. https://doi.org/10.7554/eLife.42166
40. Tegunov D, Cramer P (2018) Real-time cryo-EM data pre-processing with warp. Nat Methods 16(11):1146-1152. https://doi.org/10.1038/s41592-019-0580-y
41. Punjani A, Rubinstein JL, Fleet DJ, Brubaker MA (2017) cryoSPARC: algorithms for rapid unsupervised cryo-EM structure determination. Nat Methods 14:290–296. https://doi.org/10.1038/nmeth.4169
42. Wagner T, Merino F, Stabrin M, Moriya T, Antoni C, Apelbaum A, Hagel P, Sitsel O, Raisch T, Prumbaum D, Quentin D, Roderer D, Tacke S, Siebolds B, Schubert E, Shaikh TR, Lill P, Gatsogiannis C, Raunser S (2019) SPHIRE-crYOLO: a fast and accurate fully automated particle picker for cryo-EM. Commun Biol 2:218
43. Mastronarde DN (2005) Automated electron microscope tomography using robust prediction of specimen movements. J Struct Biol 152:36–51. https://doi.org/10.1016/j.jsb.2005.07.007
44. Palovcak E, Wang F, Zheng SQ, Yu Z, Li S, Betegon M, Bulkley D, Agard DA, Cheng Y (2018) A simple and robust procedure for preparing graphene-oxide cryo-EM grids. J Struct Biol 204:80–84. https://doi.org/10.1016/j.jsb.2018.07.007
45. Fernández-Tornero C, Moreno-Morcillo M, Rashid UJ, Taylor NMI, Ruiz FM, Gruene T, Legrand P, Steuerwald U, Müller CW (2013) Crystal structure of the 14-subunit RNA polymerase I. Nature 502:644. https://doi.org/10.1038/nature12636
46. Engel C, Sainsbury S, Cheung AC, Kostrewa D, Cramer P (2013) RNA polymerase I structure and transcription regulation. Nature 502:650. https://doi.org/10.1038/nature12712
47. Dubochet J, Adrian M, Chang JJ, Homo JC, Lepault J, McDowall AW, Schultz P (1988) Cryo-electron microscopy of vitrified specimens. Q Rev Biophys 21:129–228
48. Russo CJ, Scotcher S, Kyte M (2016) A precision cryostat design for manual and semi-automated cryo-plunge instruments. Rev Sci Instrum 87:114302. https://doi.org/10.1063/1.4967864